Published in final edited form as:

RSC Adv. 2016 ; 6(36): 30285–30292. doi:10.1039/C6RA06798K.

ICG-conjugated Magnetic Graphene Oxide for Dual Photothermal and Photodynamic Therapy

Ismail Ocsoy[1,2,3], **Nuran Isiklan**[4], **Sena Cansiz**[1], **Nalan Özdemir**[5], and **Weihong Tan**[1]

[1]Center for Research at the Bio/Nano Interface, Department of Chemistry and Shands Cancer Center, UF Genetics Institute and McKnight Brain Institute, University of Florida, Gainesville, Florida, 32611

[2]Department of Analytical Chemistry, Faculty of Pharmacy, Erciyes University, Kayseri, 38039 Turkey

[3]Nanotechnology Research Center (ERNAM), Erciyes University, Kayseri, 38039 Turkey

[4]Department of Chemistry, Science and Arts Faculty, Kırıkkale University, Kırıkkale, 7100 Turkey

[5]Department of Chemistry, Faculty of Science, Erciyes University, Kayseri, 38039 Turkey

Abstract

Aptamer-functionalized magnetic graphene oxide conjugates loaded with indocyanine green (ICG) dye, or Apt@ICG@mGO, have been successfully developed for dual-targeted photothermal and photodynamic therapy. In general, a drug or its carrier or their dosage can be imprtant important issues in terms of toxicity. However, in this system, each component used is quite safe, biocompatibe and clean. For instance, ICG, a Food and Drug Administration (FDA) approved near-infrared (NIR) dye, serves as both a photothermal and photodynamic agent. It is immobilized on the surface of mGO via a physical interaction called "**π-π** stacking". The mGO, as a most biocomptible member of the carbo family, is selected for use as a platform for aptamer and ICG dye conjugation, as well as as a photothermal agent. The light in the near-infrared region (NIR) was chosen as a harmless light source for activating the agents for photothermal therapy (PTT) and photodynamic therapy (PDT). The magnetic properties of mGO are also used for separation of Apt@ICG@mGO conjugates from the reaction medium. Aptamer sgc8 acts as a targeting ligand to selectively and specifically bind to a protein on the membrane of cancer cell line CCRF-CEM. After the aptamer- functionalized ICG@mGO conjugates are incubated with target CEM cells at 37 °C for 2 hours, they are bound to cells or they may be internalized into the cell via endocytosis. More significantly, we demonstrated that the Apt@ICG@mGO conjugates produce heat for photothermal therapy (PTT) and singlet oxygen for photodynamic therapy (PDT) upon NIR laser irradiation at 808 nm. Thus, remarkably efficient cancer cell destructions with ~41% and ~60% and ~82% cell killing using 10, 50 and 100 ppm Apt@ICG@mGO, respectively are achieved in 5 min light exposure.

Correspondence to: Ismail Ocsoy; Weihong Tan.

†Electronic Supplementary Information (ESI) available: [TEM images of mGO, ICG concentration-dependent absorption spectra and RNO absorption spectra recorded after time increments of NIR laser irradiation].

Graphical Abstract

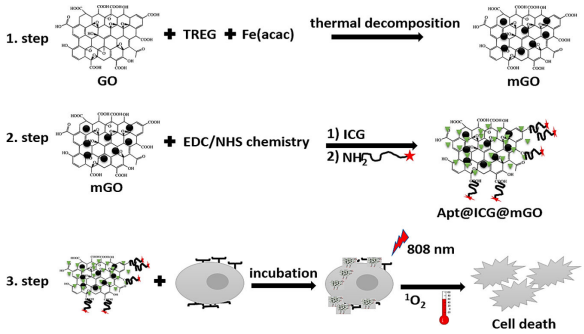

Introduction

Over the past two decades, nanoparticles (NPs) have been widely used as a platform in biomedicine based on their ability to incorporate multiple functions into a single system.[1-10] For example, plasmonic, magnetic, mesoporous, polymeric and carbon-based NPs have all been utilized to bring together multiple therapeutic models, including imaging (optical and magnetic resonance), therapy (chemo, photothermal and photodynamic), delivery (drug and gene), proteomics and biosensing. The suitability of NPs for biomedical applications depends on their level of cytotoxicity.[11-14] In particular, NPs have been used as agents to enhance therapeutic efficiency in phototherapies, particularly photothermal therapy (PTT) and photodynamic therapy (PDT), which have also been used as alternatives to chemotherapy.

In PTT, certain NPs, such as gold nanorods,[15-18] nanoshells,[19,20] nanocages,[21,22] nano-popcorns,[23] carbon nanohorns[24] and graphene[25,26] have been employed as photothermal agents. They efficiently absorb light in the near-infrared region (NIR) and rapidly convert it into heat. Eventually, this rapid local temperature increase in the microenvironment induced by NIR irradiation results in irreversible cell damage and cell death in the range of 42 and 47°C.[27]

PDT, also known as light-activated therapy, is a noninvasive medical model that causes cell destruction in the presence of reactive oxygen species (ROS), such as singlet oxygen, generated by irradiation of a photosensitizer (PS).[28-30] In PDT, PS molecules are irradiated with light at an appropriate wavelength, and the excited PS transfers photon energy to surrounding oxygen molecules to generate highly reactive singlet oxygen. The singlet oxygen molecule, as a cytotoxic agent, attacks target cells and induces irreversible damage. Both PTT and PDT have several advantages over conventional chemotherapy because they are noninvasive, selective, and relatively inexpensive, have reproducible properties and avoid the related side effects of other therapies. [28,31]

Indocyanine green (ICG) is an amphiphilic, tricarbocyanine dye, which has been approved by the United States Food and Drug Administration (FDA) for biomedical applications. Its low toxicity and unique optical properties, including its very strong absorption band (780 nm) and effective emission band (800-820 nm), make ICG ideally suited for optical imaging

in cells, tissues and small animals.[32-33] In the visible region, cell and tissue auto-fluorescence results in weak signal-to-noise ratios in vitro and in vivo, and is thus a major drawback for the generation of high-resolution optical imaging. In contrast, the use of ICG as a NIR agent is vitally important to optical imaging of human vasculature, tissue and cells, which are relatively transparent to NIR radiation (700-1300 nm), allowing deep light penetration up to several centimeters in biological tissues. Recently, ICG has also been used as a PTT and PDT agent for clinical treatment.[28-30] When ICG is irradiated with an appropriate wavelength, it can generate heat for PTT and singlet oxygen for PDT. However, the efficient use of ICG is very limited as a result of the intrinsic disadvantages associated with concentration-dependent aggregation in aqueous solution, such as easy chemical degradation, depending on the nature of the solvent, dye concentration, temperature and light exposure, and the extremely rapid pharmacokinetics of ICG and its nonspecific binding to proteins, including human serum albumin, lipoproteins, plasma proteins and endothelial cells.[37,38]

Since its discovery in 2004, graphene, which is composed of one or few atom-thick two-dimensional (2D) sp^2-bonded carbon sheets, has been extensively used in a broad spectrum of applications owing to its unique physicochemical, mechanical and electronic properties.[39] Recently, graphene oxide (GO), the oxidized form of graphene, has been utilized to construct optical, electrical and electrochemical biosensors and to design surface-enhanced Raman scattering (SERS) platforms, in addition to its use as a substrate for matrix-assisted laser desorption/ionization (MALDI), antimicrobial agent[40, 41] and as a carrier for drug and DNA delivery.[42-46] The large surface area of GO, which features many functional groups and domains, as well as its biocompatibility, make GO an ideal platform for efficient conjugation of aromatic biomolecules, such as anticancer drugs, photosensitizers, proteins, peptides and single-stranded DNA, through **π-π** stacking. Recently, ‘pi-excessive’ or ‘electron-rich’ drugs and photosensitizers have been efficiently loaded on the surface of GO for chemo- and photodynamic therapies.[47,48] For instance, Dai and coworker reported on water-insoluble anticancer drugs physically loaded on the GO surface for effective chemotherapy.[49] Loading of two anticancer drugs on the GO surface was achieved by Zhang and coworkers, who used GO functionalized with folic acid to convey two water-insoluble cancer drugs, camptothecin and doxorubicin, to specifically treat MCF-7 human breast cancer cells.[41] Recent reports also demonstrate that GO can act as a photothermal agent for medical treatment.[50-53]

Aptamers, a new class of targeting ligands, have been selected and amplified for specific targets. A wide range of targets, including metal ions (Pb^{2+}, Cd^{2+}), small molecules (cocaine, adenosine triphosphate), proteins (protein tyrosine kinase 7, immunoglobulin G, nucleolin and thrombin) and even whole viruses (human influenza B), bacteria (Methicillin-resistant Staphylococcus aureus (MRSA)) and cancer (T-cell acute lymphoblastic leukemia, B lymphocyte and MCF-7 human breast cancer) cells, has been used to generate single-stranded DNA- or RNA-based aptamers by a process termed “SELEX” (Systematic Evolution of Ligands by Exponential enrichment) with dissociation constants (Kd) in the micromolar to nanomolar (nM), or even picomolar (pM), ranges.[54-62] Aptamers have received considerable attention by bioscience researchers because of their exceptional properties, including flexibility, reproducibility in the selection and synthesis protocol, low

molecular weight, low immune response, reversible denaturation, easy chemical modification, and stability.[63] Tan and coworkers have isolated and identified aptamers using whole living cells via a new technique known as cell-SELEX, which produces aptamers that bind with high affinity and selectivity to receptors, typically a protein, on the membranes of target cells. Thus, early diagnosis and targeted therapy have been successfully accomplished by using aptamer recognition of molecular signatures on target cells.[53,57]

In this work, we developed a multifunctional hybrid nanostructure capable of providing targeted PTT and PDT. First, we synthesized magnetic graphene oxide (mGO) to utilize as a platform for loading ICG dye via **π-π** stacking. Then, the edges of mGO were functionalized with sgc8 DNA aptamers as targeting ligands for binding to target cells. Magnetic-GO and ICG have been separately considered as photothermal agents. With NIR light irradiation, Apt@ICG@mGO exhibits a cooperative effect by generating high local heat reaching 43°C in 20 seconds. However, ICG, as a PDT agent, also produces singlet oxygen under NIR laser irradiation. Thus, the combination of PTT and PDT enhances target cancer cell killing efficiency. Our results show the Apt@ICG@mGO conjugate to be a promising nanostructure system for effective light-induced cancer cell destruction by enhanced PTT and PDT.

Result and discussion

The aptamer-functionalized Apt@ICG@mGO conjugates developed in this study act as a highly biocompatible and water-soluble platform for targeted PTT and PDT. First, GO nano powder in TREG was homogeneously dispersed by ultrasonication. Subsequently, $Fe(acac)_3$ used as iron precursor was added to the mixture, and it was refluxed at 278°C for 60 min to form magnetic Fe_3O_4 NPs on the surface of GO. The density of Fe_3O_4 NPs on the GO surface was controlled by adjusting the weight ratio of $Fe(acac)_3$ and GO. Attaching ICG to the surface of mGO was achieved by **π-π** stacking interactions. The synthesis of mGO , Apt@ICG@mGO and their with cells and cell destruction via PTT and PDT are both depicted in **Fig. 1**. EDC/NHS chemistry was utilized to activate the carboxyl groups located at the edges of mGO dispersed in 10 mM PBS solution (pH 7.4), resulting in the binding of NH_2-group-labeled sgc8 aptamers to the activated carboxyl groups. Several reports already stated that the presence of carbonyl groups located at the edges as the dominant functional groups.[64-67] The Apt@ICG@mGO conjugates were then incubated with about 10^6 cancer cells for 2h at 37°C for surface biding or internalization.

GO, mGO and ICG@mGO were characterized via transmission electron microscopy (TEM), Fourier transform infrared spectroscopy (FTIR) and UV-vis spectrometry. Fig. 2A shows the TEM image of bare GO in pieces of various sizes. Fe_3O_4 NPs grown on GO (1:1 weight ratio) were clearly observed by TEM (Fig. 2B). The different weight ratios of $Fe(acac)_3$/GO nano powder (5:1, 4:1 and 2:1) changed the number of Fe_3O_4 NPs on the surface of GO (Fig. S1 in the Supplementary data). The color of GO in aqueous solution was brown (Fig. 2C (i)), while the color of mGO became black after formation of Fe_3O_4 NPs on the surface of GO (Fig. 2C (ii)). The photograph in Fig. 2C (ii) also shows that mGO is highly water-soluble and stable in aqueous solution without any aggregation. The mGO dispersed in PBS solution was accumulated on the wall of a glass vial, demonstrating the magnetic property of

mGO (Fig. 2C (iii)). It should be noted that accumulated mGO remained on the vial wall for a long time, even after the external magnetic field (magnet) was removed (Fig. 2C (iv)).

Free ICG with various concentrations dissolved in ethanol or water exhibited a characteristic absorption peak around 780 nm (Fig. 2D). Free ICG in aqueous solution forms aggregates in a short time, depending on its concentration, and it is also rapidly degraded. ICG at low concentrations (≤129 μM) exhibits single or double sharp absorption peak(s), while concentrations of ICG greater than129 μM show a very broad peak between 780 and 590 nm, which is also an indication of agglomeration of ICG monomers (Fig. S2 in the Supplementary data). After loading ICG on the mGO surface via pi-electron delocalization, a characteristic peak of ICG appeared around 808 nm (28 nm red shift), which matched the wavelength of the NIR laser used for PTT and PDT (Fig. 2D). In addition, mGO was used as both carrier and stabilizer to prevent aggregation of ICG. FTIR spectra were obtained for ICG and ICG@mGO (Fig. 2E). For mGO, the O-H stretching vibration appeared at 3437 cm^{-1}, and aromatic C=C and carboxyl stretching vibrations appeared at 1599cm^{-1} and 1384 cm^{-1}, respectively. The vibration of C-O in the epoxy group appeared at 1114 cm^{-1}. For ICG@mGO, the vibrational stretching of C=N and C=C appeared at 1602 cm^{-1} and 1414 cm^{-1}, respectively, while the vibrational stretching of single-bond C-N appeared at 1352 cm^{-1}. All of these stretching vibrations were present in ICG. The stretching vibrations of S=O (1089 cm^{-1}), C-S and S-O (1089 cm^{-1}) were also indications of successful conjugation of ICG on the surface of mGO. Carbon–oxygen vibration (C–O–C) at 854 and 1088 cm^{-1} appeared.

Singlet oxygen generation ($^1O_2$) is a key component for PDT. The extent of $^1O_2$ produced by free ICG and ICG@mGO was determined on the basis of decreased absorbance of N,N-dimethyl-4-nitrosoaniline (RNO) via UV-vis spectroscopy. The mixture of free ICG and RNO was irradiated with the 808 nm NIR laser, and the absorbance of RNO at 440 nm decreased as a result of $^1O_2$ production (Fig. 3A). When the mixture of mGO and RNO was exposed to NIR laser irradiation, the generation of $^1O_2$ was not observed (Fig. 3B). Although mGO almost completely quenched the fluorescence of ICG loaded on its surface in the ICG@mGO conjugate, it is interesting that ICG was still partially capable of producing $^1O_2$ under NIR laser irradiation (Fig. 3C). This can be explained by the structural differences of GO compared to other carbon-based materials. For instance, GO may have surface defects, which cause slight energy absorption. We proved that RNO itself did not generate any $^1O_2$, even though it was exposed to NIR laser irradiation for 10 min (Fig. S3 in the Supplementary data). Note that ICG and ICG@mGO without light irradiation were unable to generate $^1O_2$, as shown by the red line in Fig. 3A and 3C. Furthermore, the fluorescence spectra of ICG and ICG@mGO showed fluorescence interaction between ICG and mGO. More than 95% of ICG fluorescence was quenched after it was loaded on the surface of mGO (Fig. 3D).

To show the heat generation capability of mGO, free ICG and ICG@mGO, each material was dissolved in PBS solution and irradiated with the 808 nm laser for 5 min (Fig. 4). The mGO (50μg mL^{-1}) caused an increase in temperature from ~24°C to ~58°C within 5 min, while free ICG solution (5 μM) reached ~54°C. However, the ICG@(5μM)mGO (50μg mL^{-1}) conjugate dramatically increased the temperature from ~24°C to ~76°C. Within 40 s,

we observed that the ICG@mGO conjugate reached ~51°C, which can destroy all types of cancer cells. We conclude that the ICG@mGO conjugate causes a temperature increase greater than that of either mGO or free ICG alone. We speculate that the 28 nm shift in the λmax of ICG to 808 nm, as shown Fig. 2D, provided rapid and abundant heat production.

Binding of Apt@ICG@mGO to the target CCRF-CEM cells was performed at 37°C for 2h (Fig. 5A). First, one million CCRF-CEM cells were prepared in seven separate tubes. Tube 1 contained only cells without any aptamer or hetero-nanostructures, while tubes 2 and 3 were mixed with free library DNA and sgc8 aptamer, respectively. Tube 4 contained only ICG@mGO without aptamer, while tubes 5, 6, and 7 included Apt@ICG@mGO conjugates with respective concentrations of 10, 100 and 200 ng mL^{-1}. All tubes were incubated in an incubator shaker at 250 rpm (Forma Refrigerated Orbital Shaker, Thermo Electron Corp., Asheville, NC, USA) at 37°C for 2 h. After incubation, the contents of each tube were washed with washing buffer and redispersed in binding buffer prior to flow cytometry. The fluorescence signal, as an indication of cell binding and internalization, was not observed with cells only (red line). The FTIC-labeled library DNA used as a control did not show any binding to target cells, as expected (light green line). However, a significant right shift was observed with the mixture of cells and FITC-labeled sgc8 aptamer because this aptamer specifically bound and entered the target cells (blue line). No binding or internalization was observed with ICG@mGO conjugates without aptamer. In contrast, sgc8 aptamer-functionalized ICG@mGO conjugates resulted in successful binding and internalization. Furthermore, the fluorescence signal intensities, as right shifts, increased with increasing concentrations of sgc8 Apt@ICG@mGO conjugates from 10ng mL^{-1}(brown line) to 100 ng mL^{-1} (dark green) and 200 ng mL^{-1} (orange line).

To assess the efficiency of PTT and PDT, cell viability tests were performed with only cells (a), mGO (b), free ICG (c), ICG@mGO (d), Sgc8@mGO (e), Sgc8@ICG@mGO (f) and rDNA@ICG@mGO (g) (10, 50, 100 ppm) under nonilluminated and illuminated conditions. It is worthy to mention that the light activates both PTT and PDT agents (GO and ICG) which kills the cancer cells. Without light, these biocompatible agents are harmless. Target CCRF-CEM cells were separately incubated with each structure aforementioned, followed by non-irradiation and 808 nm laser irradiation at 1.1 W cm^{-2} for 5 min, respectively. The mGO, utilized as photothermal agent, generated heat for PTT. However, the ICG@mGO conjugate served as both a photothermal and a photodynamic agent owing to the presence of ICG. Thus, the enhanced PTT, based on the heat generated both from ICG and mGO, and PDT, based on the production of $^1O_2$ by ICG, led to effective destruction of target cancer cells. However, the regardless of structures and their dosages, there was no reduction in the number of live cancer cells under the nonilluminated condition (without 808 nm laser irradiation) as shown in Fig. 5B. In contrast to that, when 808 nm NIR laser irradiation was exposed to structures for 5 min, the cancer cell destruction was observed (Fig. 5C). Although only cell solution was illuminated with NIR laser, no cell destruction was seen due to absence of structures generating heat or $^1O_2$.

For instance, when NIR laser irradiation was introduced, mGO conjugates only killed ~9% and ~13% and ~20% of cell with respective concentrations (10, 50 and 100 ppm) while free ICG induced ~6% and ~11% and ~17%. However, a slight increase in cell killing stated (7%

and ~19% and ~24% when ICG@mGO conjugated used. None of these conjugates was not functionalized with aptamer, due to that they were lack of binding target cell. After incubation of the mixture of target cell and these conjugates, the most of conjugates were removed from the mixture by centrifugation except a little amount of nonspecifically binding one. The aptamer functionalized sgc8@mGO decreased the survival rate of CCRFCEM cells by killing ~32%, ~40% and ~50% of CCRF-CEM cells at 10, 50 and 100 ppm, respectively while sgc8@ICG@mGO showed dramatic reduction in cell viability with 41%, ~60% and ~82% (Fig. 5C). To prove the function of aptamer for enhancing the cell-killing ability of conjugates, we also immobilized ICG@mGO with random DNA (rDNA@ICG@mGO). We demonstrated that rDNA@ICG@mGO only killed ~21% of CCRF-CEM cells at 100 ppm. This result also support function and importance of aptamer for targeting target cell. We conclude that the rapid increase in heat generated from both ICG and mGO and generation of $^1O_2$ from ICG components of ICG@mGO conjugates combined with targeting capability of sgc8 aptamer the resulted in enhanced dual PT and PD therapies for effectively and rapidly killing of CCRF-CEM cells.

Conclusions

In this work, we developed multifunctional aptamer-functionalized ICG-loaded mGO for enhanced photothermal and photodynamic therapy. The sgc8 aptamer, as a targeting ligand, bound with high affinity and selectivity to CCRF-CEM cancer cells for targeted therapy. By utilizing mGO as both a platform for aptamer functionalization and a carrier for ICG loading via pi-pi stacking, the photothermal heating property of mGO was realized. In addition, ICG served as both a photothermal and photodynamic agent for heat and singlet oxygen generation, respectively. Although ICG loaded on the surface of mGO generated less singlet oxygen compared to free ICG, the cancer cells were efficiently killed through the photodynamic process as a result of binding of ICG via sgc8 targeting. Apt@ICG@mGO conjugates in this study offered enhanced PTT and PDT for efficient cancer cell destruction when irradiated with the 808 nm NIR laser. Therefore, the unique NIR absorption property of ICG and mGO makes Apt@ICG@mGO an ideal candidate for effective PTT and PDT, suggesting the further use of mGO in biomedical applications based on its nontoxicity and unique capability to load aromatic molecules.

Experimental

All chemicals were used as received without further purification. Nano graphene oxide powder (100 mg) (GO) with sizes ranging from 100 nm to 500 nm was purchased from the Graphene Supermarket (Ronkonkoma, NY). Indocyanine green dye (cardiogreen), triethylene glycol (TREG), iron (III) acetylacetonate ($Fe(acac)_3$), N,N-dimethyl-4-nitrosoaniline (RNO), 1-ethyl-3-(3-dimethylaminopropyl) carbodiimide (EDC) and N-hydroxy succinimide (NHS) were purchased from Sigma-Aldrich. Salts (NaCl, KCl, Na_2HPO_4, KH_2PO_4, $CaCl_2$. $2H_2O$, and $MgCl_2{\cdot}6H_2O$) were also purchased from Sigma-Aldrich. Ultrapure water (18.2 MΩ; Millipore Co., USA) was used in all experiments.

Instrumentation and characterization

Transmission electron microscopy (TEM) (Hitachi H-7000) with a working voltage of 100 kV was used to generate images of GO and mGO. For sample preparation, a few drops of GO and mGO nanostructures dispersed in water were deposited on carbon-coated copper grids and left overnight to completely dry. The absorption spectra of ICG, GO, mGO and aptamer-ICG@mGO were obtained using an 1800 UV-vis spectrophotometer (Shimadzu Scientific Instruments, Columbia, MD). ICG and ICG@mGO were also characterized by FTIR analysis (near and mid IR Nicolet Nexus 670). The ICG and ICG@mGO powders were separately mixed with potassium bromide (KBr) powder (transparent in the mid-IR region), and then the mixtures were ground and pressed to obtain very thin plates. The plates were placed in the sample holder for FTIR analysis. The concentrations of DNA aptamer and library were determined using the same UV-vis spectrophotometer. Emission spectra of ICG and dye-labeled DNA aptamer were produced by a Fluoromax-4 (Horiba Jobin-Yvon, Edison, NJ, USA). Binding of aptamer-ICG@mGO to the target cancer cells was demonstrated with a FACScan cytometer (Becton Dickinson Immunocytometry Systems, San Jose, CA, USA).

Cell lines

CCRF-CEM cells (CCL-119 T-cell, human acute lymphoblastic leukemia) were purchased from ATCC (American Type Culture Collection). RPMI medium containing 10% fetal bovine serum (FBS) and 100 IU/mL penicillin-streptomycin was used for cell culture (5% CO2, at 37°C). The cell density prior to experiments was determined by a hemocytometer. Approximately one million cells were suspended in RPMI cell media and centrifuged at 1200 rpm for 3 min. After this, cells were resuspended in 2 mL washing buffer (Dulbecco's PBS with calcium chloride and magnesium chloride supplemented with 4.5 g/L glucose and 5 mM $MgCl_2$) for incubation.

Synthesis of aptamers

The aptamer selected for the CCRF-CEM cells, sgc8c, (5′-FTIC-ATC TAA CTG CTG CGC CGC CGG GAA AAT ACT GTA CGG TTA GA-NH2-3) and library DNA containing a randomized sequence of 41 nucleotides were synthesized at a μmol scale using an ABI3400 DNA/RNA synthesizer (Applied Biosystems, Foster City, CA). Both sgc8c and DNA library were coupled with fluorescein isothiocyanate dye (FTIC) modifier at the 5’ end and amine (-NH_2) modifier at the 3’ prime end during synthesis. After synthesis, they were deprotected in AMA (ammonium hydroxide /40% aqueous methylamine, 1:1) at 65°C for 30 min. After deprotection, all sequences were purified by reversed-phase HPLC (ProStar-Varian, Walnut Creek, CA) with a C18 column (Econosil, 5μm, 250mm length, 4.6mm diameter) from Alltech (Deerfield, IL) using a mobile phase containing 100 mM triethylamine acetic acid buffer (TEAA, pH 7.5) and acetonitrile (0-30min, 10-00%). All purified DNA solutions were dried in acid-resistant centriVap centrifugal vacuum concentrators (Labconco, Kansas City, MO). The dried DNA at the bottom of 2 mL tubes was dissolved in 50-100μL of DNA grade water. The concentrations of all DNA were determined by measuring the absorbance values at 260 nm.

Synthesis of magnetic graphene oxide nanostructures

The synthesis of mGO was accomplished using a modified method.[68] Twenty mg GO nano powder was added to a 30 mL glass vial containing 20 mL triethylene glycol (TREG), and then the mixture was subjected to ultrasonication for 40 min until the GO nano powder was homogeneously dispersed in TREG. The resultant mixture was transferred to a 100 mL flask, and 30 mg $Fe(acac)_3$ was added. The final mixture was vigorously stirred until $Fe(acac)_3$ was completely dissolved. Then it was slowly heated to 278°C for refluxing with vigorous stirring. After refluxing for 60 min, the mixture was allowed to cool to room temperature with stirring in an argon atmosphere. The product was magnetically isolated by an external magnet and washed at least three times with ethanol to remove excess solvent and unreacted components. Finally, the collected product was placed in vacuum to dry at 60°C. The density of iron oxide nanoparticles formed on the surface of mGO was adjusted by manipulating the weight ratio between $Fe(acac)_3$ and GO powder.

Loading ICG on the surface of magnetic graphene oxide nanostructures

In order to adsorb ICG on the surface of mGO, 1mL of 200 μg mL^{-1} mGO in water was mixed with 1mM ICG dissolved in ethanol, and the resulting mixture was incubated at room temperature (RT) overnight. ICG-adsorbed mGO was separated by a magnet, and the supernatant containing unadsorbed excess ICG was removed and stored in a separate tube. The ICG@mGO precipitates were redispersed in water and separated again with a magnet. This washing process was repeated at least 4-5 times. The magnetic property of mGO allowed the simple removal of ICG@mGO from the reaction solution and prevented nonspecific adsorption of ICG on the mGO surface resulting from centrifugation. The collected ICG@mGO was dispersed in 10 mM PBS (pH 7.4) and used for further DNA functionalization.

Functionalization of ICG-loaded magnetic graphene oxide nanostructures

DNA aptamer (sgc8) was bound to ICG@mGO using conventional protein labeling chemistry. First, 200 μg ICG@mGO dispersed in 1 mL 10 mM PBS solution (pH 7.4) and 60μL 0.1 M 1-ethyl-3-(3-dimethylaminopropyl) carbodiimide (EDC) were mixed. The mixture was placed on a shaker (250 rpm) and incubated at RT for 30 min to activate the carboxyl groups on the edges of mGO. After incubation, 15 μL 440 μM sgc8 aptamer and 60 μL 0.12M N-hydroxysuccinimide (NHS) in 10mM PBS solution were added, followed by incubating the final mixture at 20°C for 4h under gentle shaking for functionalization of ICG@mGO with sgc8 aptamer. The sgc8 aptamer-functionalized ICG@mGO (Apt@ICG@mGO) conjugates were separated by a magnet from the reaction solution without centrifugation. The resultant product was washed three times with 10 mM PBS buffer and separated by a magnet to prevent, or minimize, nonspecific adsorption of DNA on the ICG@mGO surface. Finally, the Apt@ICG@mGO conjugates were redispersed in 600μL of 10 mM PBS solution and used for cancer cell binding and internalization studies. Detection of singlet oxygen generation: To determine the generation of singlet oxygen, known concentrations of mGO, ICG and ICG@mGO were mixed with N,N-dimethyl-4-nitrosoaniline (RNO) (20μM) and imidazole (20μM) in 1 mL 10 mM PBS solution (pH 7.4). Each resulting mixture was illuminated at 808 nm using a near-infrared (NIR) laser with

power of 1.1 W cm^{-2} for different periods of time. The reduction of RNO absorption at 440 nm indicated the generation of singlet oxygen from each sample (mGO, ICG and ICG@mGO).

Cell viability assay

The killing effect of PTT and PDT for CCRF-CEM target cells was determined by cell viability assay. Before these therapies, target cells were prepared. First, 1×106mL^{-1} CCRF-CEM cells were incubated with various concentrations of Apt@mGO and Apt@ICG@mGO (50, 100, 150 μgmL^{-1}) in 250 μL binding buffer at 37°C for 2h with a 5% CO_2 atmosphere. In order to remove unreacted components, the mixtures were washed with washing buffer at least twice. The cell mixtures were irradiated by 808 nm NIR laser for 5 min and placed in the incubator at 37°C for 48 h. The standard MTT assay was carried out to determine cell viability by comparing cells treated with Apt@mGO and Apt@ICG@mGO.

PTT and PDT under NIR laser irradiation

The λmax of free ICG dissolved in ethanol or water is 780 nm. However, after ICG was loaded on mGO surface, the λmax shifted to 808 nm, which matches the NIR laser wavelength used for PTT and PDT. The mGO absorbs light in the visible and NIR regions. The temperature curves generated from mGO and ICG@mGO were recorded in real time by using a COHERENT Quarto-FAP system. The cell mixtures were irradiated by a continuous wave laser (808 nm) with power density of 1.1 W cm^{-2} for 5 min.

Supplementary Material

Refer to Web version on PubMed Central for supplementary material.

Acknowledgements

This work is supported by grants awarded by the National Institutes of Health (GM079359 and CA133086). The authors sincerely thank Dr. Kathryn Williams for assistance with manuscript revision and John W. Munson in the Center for Environment and Human Toxicology (CEHT) at the University of Florida for laser support.

References

1. Wang X, Han Q, Yu N, Li Jing, Yang L, Yang R, Wang C. J. Mater. Chem. B. 2015; 3:4036–4042.
2. Nellore BPV, Pramanik A, Chavva SR, Sinha SS, Robinson C, Fan Z, Kanchanapally R, Grennell J, Weaver I, Hamme AT, Ray PC. Faraday Discuss. 2014; 175:257–271. [PubMed: 25277344]
3. Huang P, Xu C, Lin J, Wang C, Wang X, Zhang C, Zhou X, Guo S, Cui D. Theranostics. 2011; 1:240–250. [PubMed: 21562631]
4. Tao Y, Ju E, Ren J, Qu X. Biomaterials. 2014; 35:9963–9971. [PubMed: 25224368]
5. Shibua ES, Hamadaa M, Murasea N, Biju V. J. Photochem. Photobiol. 2013; 15:53–72.
6. Yang Z-Y, Li H, Zeng Y-P, Hao Y-H, Liu C, Liu J, Wang W-D, Li R. ACS Appl. Mater. Interfaces. 2015; 7:24218–24228. [PubMed: 26485120]
7. Maeng JH, Lee DH, Jung KH, Bae YH, Park IS, Jeong S, Jeon YS, Shim CK, Kim W, Kim J, Lee J, Lee YM, Kim JH, Kim WH, Hong SS. Biomaterials. 2010; 31:4995–5006. [PubMed: 20347138]
8. Park H, Yang J, Lee J, Haam S, Choi IH, Yoo KH. ACS. Nano. 2009; 3:2919–2926. [PubMed: 19772302]
9. Lee SM, Park H, Yoo KH. Adv. Mater. 2010; 22:4049–4053. [PubMed: 20665571]
10. Ma X, Zhao Y, Liang XJ. Acc. Chem. Res. 2011; 44:1114–1122. [PubMed: 21732606]

11. Hu R, Zhang XB, Kong RM, Zhao XH, Jiang J, Tan W. J. Mater. Chem. 2011; 21:16323–16334.
12. Jain PK, Huang X, El-Sayed IH. Acc. Chem. Res. 2008; 41:1578–1586. [PubMed: 18447366]
13. Ocsoy I, Paret ML, Arslan Ocsoy M, Kunwar S, Chen T, You M, Tan W. ACS. Nano. 2013; 7:8972–8980. [PubMed: 24016217]
14. Ocsoy, Gulbakan B, Shukoor M, Xiong X, Chen T, Powell DH, Tan W. ACS. Nano. 2013; 7:417–427. [PubMed: 23211039]
15. Kuo WS, Chang YT, Cho KC, Chiu KC, Lien CH, Yeh CS, Chen SJ. Biomaterials. 2012; 33:3270–3278. [PubMed: 22289264]
16. Kuo WS, Chang CN, Chang YT, Yang MH, Chien YH, Chen SJ, Yeh CS. Angew. Chem. Int. Ed. 2010; 49:2711–2715.
17. Huang YF, Chang HT, Tan W. Anal. Chem. 2008; 80:567–572. [PubMed: 18166023]
18. Huang X, El-Sayed IH, Qian W, El-Sayed MA. J. Am. Chem. Soc. 2006; 128:2115–2120. [PubMed: 16464114]
19. Bardhan R, Chen W, Perez-Torres C, Bartels M, Huschka RM, Zhao LL, Morosan E, Pautler RG, Joshi A, Halas NJ. Adv. Funct. Mater. 2009; 19:3901–3909.
20. Bardhan R, Lal S, Joshi A, Halas NJ. Acc. Chem. Res. 2011; 44:936–946. [PubMed: 21612199]
21. Skrabalak SE, Chen J, Au L, Lu X, Li X, Xia Y. Adv. Mater. 2007; 19:3177–3184. [PubMed: 18648528]
22. Au L, Zheng D, Zhou F, Li ZY, Li X, Xia Y. ACS. Nano. 2008; 2:1645–1652. [PubMed: 19206368]
23. Lu W, Singh AK, Khan SA, Senapati D, Yu H, Ray PC. J. Am. Chem. Soc. 2010; 132:18103–18114. [PubMed: 21128627]
24. Zhang MF, Murakami T, Ajima K, Tsuchida K, Sandanayaka ASD, Ito O, Iijima S, Yudasaka M. Proc. Natl. Acad. Sci. USA. 2008; 105:14773–14778. [PubMed: 18815374]
25. Sherlock SP, Tabakman SM, Xie L, Dai H. ACS. Nano. 2011; 5:1505–1512. [PubMed: 21284398]
26. Yang Y, Asiri AM, Tang Z, Du D, Lin Y. Materials Today. 2013; 16:365–373.
27. Huang CC, Su CH, Li WM, Liu TY, Chen JH, Yeh CS. Adv. Funct. Mater. 2009; 19:249–258.
28. Lovell JF, Liu TWB, Chen J, Zheng G. Chem. Rev. 2010; 110:2839–2857. [PubMed: 20104890]
29. Dolmans DE, Fukumura D, Jain RK. Nat.Rev.Cancer. 2003; 3:380–387. [PubMed: 12724736]
30. Agostinis P, Berg K, Cengel KA, Foster TH, Girotti AW, Gollnick SO, Hahn SM, Hamblin MR, Juzeniene A, Kessel D, Korbelik M, Moan J, Mroz P, Nowis D, Piette J, Wilson BC, Golab J. CA Cancer J Clin. 2011; 61:250–281. [PubMed: 21617154]
31. Wilson BC, Patterson MS. Phys. Med. Biol. 2008; 53:R61–R109. [PubMed: 18401068]
32. Larush L, Nanomedicine S. 2011; 6:233–240.
33. Mok H, Jeong H, Kim SJ, Chung BH. Chem. Commun. 2012; 48:8628–8630.
34. Zheng X, Xing D, Zhou F, Wu B, Chen WR. Mol Pharmaceutics. 2011; 8:447–456.
35. Barth BM, Altınoğlu EI, Shanmugavelandy SS, Kaiser JM, Crespo-Gonzalez D, DiVittore NA, McGovern C, Goff TM, Keasey NR, Adair JH, Loughran TP. ACS Nano. 2011; 5:5325–5337. [PubMed: 21675727]
36. Zheng M, Yue C, Ma Y, Gong P, Zhao P, Zheng C, Sheng Z, Zhang P, Wang Z, Cai L. ACS. Nano. 2013; 7:2056–2067. [PubMed: 23413798]
37. Saxena V, Sadoqi M, Shao J. Photochem Photobiol B, Biol. 2004; 74:29–38.
38. Alander JT, Kaartinen I, Laakso A, Pätilä T, Spillmann T, Tuchin VV, Venermo M, Välisuo P. Int. J. Biomed. Imaging. 2012:940585. [PubMed: 22577366]
39. Geim AK, Novoselov KS. Nat. Mater. 2007; 6:183–191. [PubMed: 17330084]
40. Ocsoy I, Gulbakan B, Chen T, Zhu G, Chen Z, Sari MM, Peng L, Xiong X, Fang X, Tan W. Adv. Mater. 2013; 25:2319–2325. [PubMed: 23436286]
41. L Strayer A, Ocsoy I, Tan W, Jones J, Paret ML. Plant Dis. 2016 doi.org/10.1094/PDIS-05-15-0580-RE.
42. Sanchez VC, Jachak A, Hurt RH, Kane AB. Chem. Res. Toxicol. 2011; 25:15. [PubMed: 21954945]
43. Feng L, Zhang S, Liu Z. Nanoscale. 2011; 3:1252–1257. [PubMed: 21270989]

44. Zhang L, Lu Z, Zhao Q, Huang J, Shen H, Zhang Z. Small. 2011; 7:460–467. [PubMed: 21360803]
45. Sudibya HG, He QY, Zhang H, Chen P. ACS. Nano. 2011; 5:1990–1994. [PubMed: 21338084]
46. Gulbakan B, Yasun E, Shukoor MI, Zhu Z, You M, Tan X, Sanchez H, Powell DH, Dai H, Tan W. J. Am. Chem. Soc. 2010; 132:17408–17410. [PubMed: 21090719]
47. Huang P, Xu C, Lin J, Wang C, Wang X, Zhang C, Zhou X, Guo S, Cui ve D. Theranostics. 2011; 1:240–250. [PubMed: 21562631]
48. Liu Z, Robinson JT, Sun X, Dai H. J. Am. Chem. Soc. 2008; 130:10876–10877. [PubMed: 18661992]
49. Zhang L, Xia J, Zhao Q, Liu L, Zhang Z. Small. 2010; 6:537–544. [PubMed: 20033930]
50. Robinson JT, Tabakman SM, Liang Y, Wang H, Casalongue HS, Vinh D, Dai H. J. Am. Chem. Soc. 2011; 133:6825–6831. [PubMed: 21476500]
51. Li JL, Hou XL, Bao HC, Sun L, Tang B, Wang JF, Wang XG, Gu M. J. Biomed. Mater. Res A. 2014; 102:2181–2188. [PubMed: 23852749]
52. Feng L, Li K, Shi X, Gao M, Liu J, Liu Z. Adv. Healthc. Mater. 2014; 3:1261–1271. [PubMed: 24652715]
53. Gonçalves G, Vila M, Bdikin I, Andrés A, Emami N, Ferreira RAS, Carlos LD, Grácio J, Marques PAAP. Scientific Reports. 2014; 4:6735. [PubMed: 25339424]
54. Beaudry A, Joyce G. Science. 1992; 257:635–641. [PubMed: 1496376]
55. Shangguan D, Meng L, Cao ZC, Xiao Z, Fang X, Li Y, Cardona D, Witek RP, Liu C, Tan W. Anal. Chem. 2008; 80:721–728. [PubMed: 18177018]
56. Parekh P, Tang Z, Turner PC, Moyer RW, Tan W. Anal. Chem. 2010; 82:8642–8649. [PubMed: 20873781]
57. Zhang Y, Chen Y, Han D, Ocsoy I, Tan W. Bioanalysis. 2010; 2:907–918. [PubMed: 20657791]
58. Li C, Chen T, Ocsoy I, Zhu G, Yasun E, You M, Wu C, Zheng J, Song E, Huang CZ, Tan W. Adv. Funct. Mater. 2014; 24:1772–1780. [PubMed: 25530745]
59. Qiu L, Chen T, Ocsoy I, Yasun E, Wu C, Zhu G, You M, Han D, Jiang J, Yu R, Tan W. Nano Lett. 2015; 15:457–463. [PubMed: 25479133]
60. Yasun E, Kang H, Erdal H, Cansiz S, Ocsoy I, Huang Y-F, Tan W. Interface Focus. 2013; 3:1–9.
61. Chen T, Ocsoy I, Yuan Q, Wang R, You M, Zhao Z, Song E, Zhang X, Tan W. J. Am. Chem. Soc. 2012; 134:13164–13167. [PubMed: 22793667]
62. Ocsoy I, Arslan Ocsoy M, Yasun E, Tan W. Nano LIFE. 2013; 03:1–10.
63. Bunka DHJ, Stockley PG. Nat. Rev. Microbiol. 2006; 4:588–596. [PubMed: 16845429]
64. Gao W, Alemany LB, Ci L, Ajayan PM. Nat. Chem. 2009; 1:403–408. [PubMed: 21378895]
65. Lerf A, He H, Forster M, Klinowski J. J. Phys. Chem. B. 1998; 102:4477–4482.
66. Szabó T, Berkesi O, Forgó P, Josepovits K, Sanakis Y, Petridis D, Dékány I. Chem. Mater. 2006; 18:2740–2749.
67. Abdolhosseinzadeh S, Asgharzadeh H, Kim HS. Sci. Rep. 2015; 5:1–7.
68. Cong HP, He JJ, Lu Y, Yu SH. Small. 2010; 6:169–173. [PubMed: 19885891]

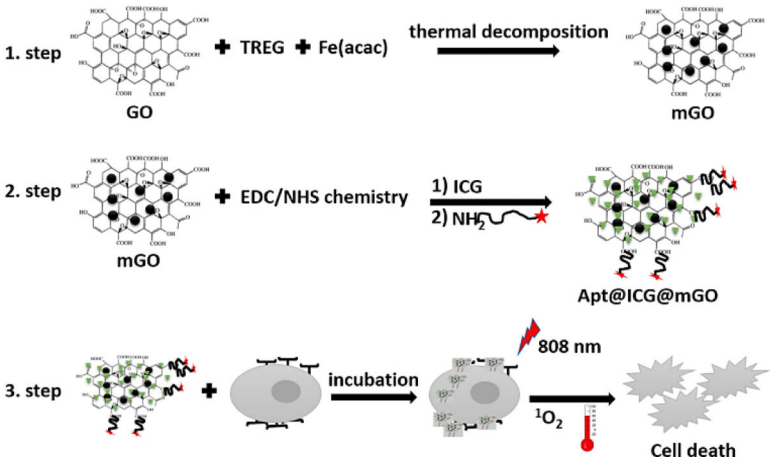

Fig.1.

Schematic illustration of synthesis of mGO, Apt@ICG@mGO and cancer cell death through PTT and PDT.

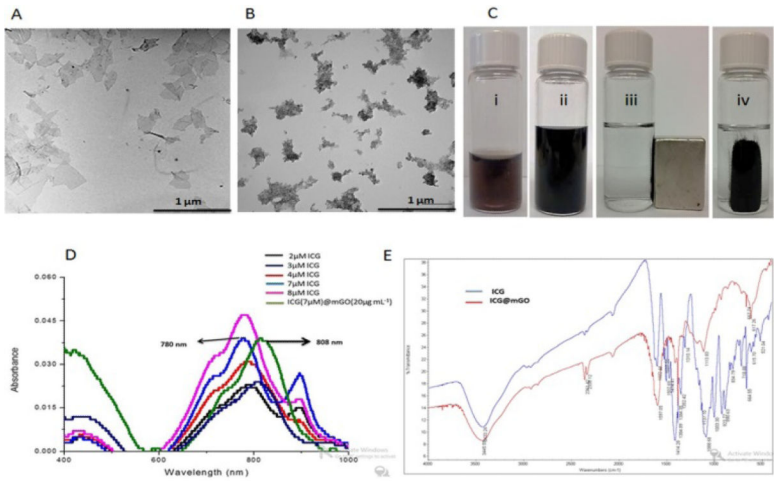

Fig. 2.

A) TEM image of bare GO, B) TEM image of mGO, C) Photograph of (i) GO, (ii) mGO, (iii), mGO with a magnet, and (iv) mGO collected on glass vial. D) UV-vis spectra of ICG and ICG@mGO; E) FTIR spectra of ICG and ICG@mGO.

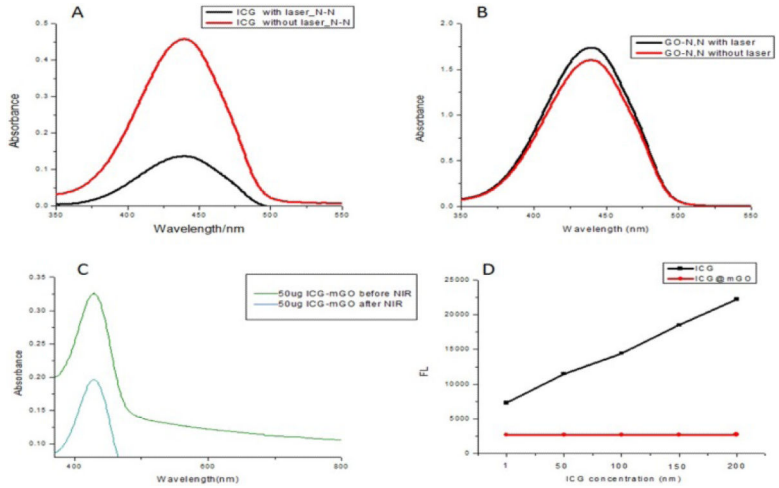

Fig. 3.

Singlet generation of A) ICG, B) GO and C) ICG@mGO. D) Fluorescence intensities of ICG and ICG@mGO at different concentrations.

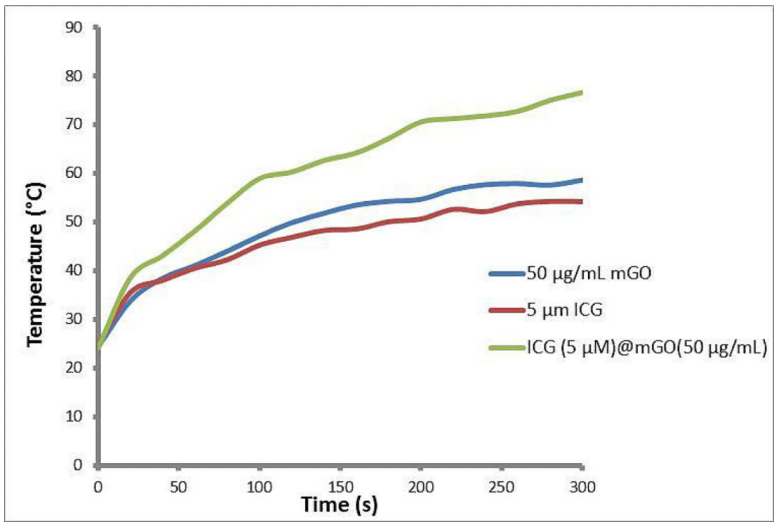

Fig. 4.

Heat generation produced by mGO, ICG and ICG@mGO. A) mGO, B) ICG, and C) ICG@mGO.

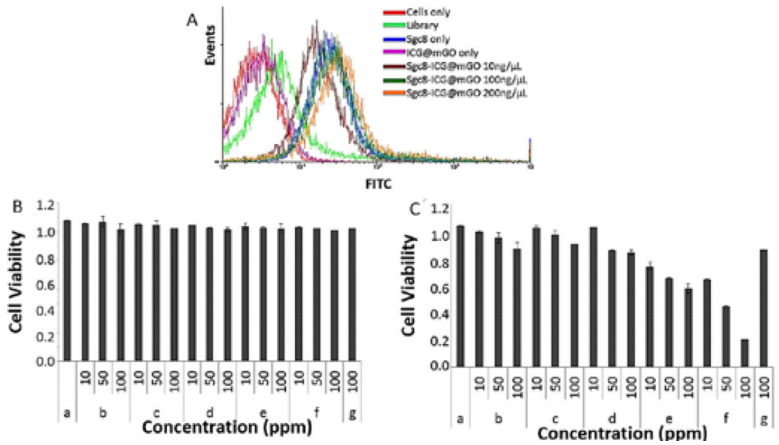

Fig. 5.

A) Flow cytometric analysis monitoring the binding of FITC-sgc8-mGO (10, 100, 200 ng/mL) to CCRF-CEM cells (target cells) at 37°C after 2 h incubation. Cell viability test. B) Under nonilluminated condition and B) under illuminated condition with 808 nm NIR laser. Only cells (a), mGO (b), free ICG (c), ICG@mGO (d), Sgc8@mGO (e), Sgc8@ICG@mGO (f) and rDNA@ICG@mGO (g).